$^{10}Be/^{9}Be$ and $^{26}Al/^{10}Be$ Support a Late Miocene Burial Age for Basal Gray Fossil Site Sediments

William E. Odom, Darryl E. Granger, and Steven C. Wallace

No. 1 Pan-American Paleontology 2025

PAN-AMERICAN PALEONTOLOGY

♦ *Pan-American Paleontology* is a peer-reviewed journal that publishes articles focusing on the paleontology of the Americas (ISSN 2475-5117 [online]). Manuscripts based on studies outside of this region that provide information on aspects of paleontology within this region may be considered at the Editor's discretion.
♦ Manuscript subject matter - The journal welcomes manuscripts based on paleontological discoveries of terrestrial, freshwater, and marine organisms and their communities. Manuscript subjects may include paleozoology, paleobotany, micropaleontology, systematics/taxonomy and specimen-based research, paleoecology (including trace fossils), paleoenvironments, paleobiogeography, and paleoclimate.
♦ It offers article-by-article online publication for prompt distribution to a global audience.
♦ It offers authors the option of publishing large files such as data tables, and audio and video clips as online supplemental files.
♦ Special issues - *Pan-American Paleontology* welcomes proposals for special issues that are based on conference proceedings or on a series of invitational articles. Special issue editors can rely on the publisher's years of experiences in efficiently handling most details relating to the publication of special issues.
♦ Indexing - *Pan-American Paleontology* is a young journal whose indexing at this time is by way of author entries in Google Scholar and Researchgate. Its indexing coverage is expected to become comparable to that of the Institute's first 3 journals (*Northeastern Naturalist*, *Southeastern Naturalist*, and *Journal of the North Atlantic*). These 3 journals are included in full-text in BioOne.org and JSTOR.org and are indexed in Web of Science (clarivate.com) and EBSCO.com.
♦ The journal's staff is pleased to discuss ideas for manuscripts and to assist during all stages of manuscript preparation. The journal has a page charge to help defray a portion of the costs of publishing manuscripts. Instructions for Authors are available online on the journal's website (http://www.eaglehill.us/papa).
♦ It is co-published with the *Northeastern Naturalist*, *Southeastern Naturalist*, *Caribbean Naturalist*, *Urban Naturalist*, *Eastern Biologist*, and *Journal of the North Atlantic*.
♦ It is available online in full-text version on the journal's website (http://www.eaglehill.us/papa). Arrangements for inclusion in other databases are being pursued.

Cover Photograph: A crew drills a core at the Gray Fossil Site, Tennessee in 2002. Photograph © S.C. Wallace.

Pan-American Paleontology (ISSN # 2475-5117) is published by the Eagle Hill Institute, PO Box 9, 59 Eagle Hill Road, Steuben, ME 04680-0009. Phone 207-546-2821 Ext. 4, FAX 207-546-3042. E-mail: office@eaglehill.us. Webpage: http://www.eaglehill.us/epal. Published on an article by article basis. **Special issue proposals are welcome**. The *Pan-American Paleontology* is an open access journal. **Authors**: Submission guidelines are available at http://www.eaglehill.us/papa. **Co-published journals:** The *Northeastern Naturalist*, *Southeastern Naturalist*, *Caribbean Naturalist*, and *Urban Naturalist*, each with a separate Board of Editors. The Eagle Hill Institute is a tax exempt 501(c)(3) nonprofit corporation of the State of Maine (Federal ID # 010379899).

$^{10}Be/^{9}Be$ and $^{26}Al/^{10}Be$ Support a Late Miocene Burial Age for Basal Gray Fossil Site Sediments

William E. Odom[1*], Darryl E. Granger[2], and Steven C. Wallace[3]

Abstract - We provide 2 independent radioisotopic age estimates for cored basal sediments of the Gray Fossil Site using cosmogenic nuclides. The first estimate uses meteoric $^{10}Be/^{9}Be$ from the bottom of the GFS-1 core, as well as from modern local grasses, to constrain the deposition of basal GFS sinkhole complex sediments to 6.60 ± 0.85 Ma. We corroborated this age estimate using *in-situ* ^{10}Be and ^{26}Al in quartz sands from the GFS-1 core. This estimate provided a looser constraint than the $^{10}Be_{met}/^{9}Be$ approach, yielding a minimum burial age for the basal sediments of 4.43 ± 0.34 Ma. These independent geochronometers provide evidence that the deepest GFS sediments are at least early Pliocene in age, and likely date to the late Miocene.

Introduction

The Gray Fossil Site (GFS) is a sinkhole complex located in Washington County, Tennessee (36.3859°N, 82.4987°W), that was discovered in 2000 during a Tennessee Department of Transportation (TDOT) construction project. It was subsequently preserved because it hosts a notably diverse late Cenozoic fossil assemblage in eastern North America, including fungi (Worobiec et al. 2018), plants (Gong et al. 2010; Hermsen 2021, 2023; Huang et al. 2014, 2015; Jiang and Liu 2008; Liu and Jacques 2010; Liu and Quan 2019; Ochoa et al. 2012; Quirk and Hermsen 2020; Siegert and Hermsen 2020; Worobiec et al. 2013; Zobaa et al. 2011), amphibians (Boardman and Schubert 2011; Gunnin et al. 2025), reptiles (Bourque and Schubert 2015; Jasinski 2018, 2022; Jasinski and Moscato 2017; Jurestovsky 2021; Mead et al. 2012; Parmalee et al. 2002), birds (Steadman 2011), and mammals (Czaplewski 2017; DeSantis and Wallace 2008; Doughty et al. 2018; Hulbert et al. 2009; Oberg and Samuels 2022; Samuels et al. 2018; Samuels and Schap 2021; Short et al. 2019; Wallace 2004, 2011; Wallace and Lyon 2022; Wallace and Wang 2004). Though the GFS hosts numerous late Neogene flora and fauna whose presence provides important evidence for interpreting climate and species patterns during this time (e.g., DeSantis and Wallace 2008; Fulwood and Wallace 2015; Liu and Quan 2019; Maclaren et al. 2018; McConnell and Zavada 2013; Ochoa et al. 2012; Schap et al. 2021; Schap and Samuels 2020; Wallace 2004, 2011; Wallace and Lyon 2022; Wallace and Wang 2004), the precise age of the site has only been proposed using biostratigraphy, with somewhat conflicting age estimates derived from mammals (e.g., Samuels et al. 2018, Samuels and Schap 2021, Wallace and Wang 2004) and fossil pollen (e.g., Zobaa et al. 2011). Using *in-situ* and meteoric cosmogenic nuclide geochronology, we provide 2 independent radiometric ages for the filling of the GFS sinkhole complex.

---

[1]U.S. Geological Survey, Florence Bascom Geoscience Center, 12201 Sunrise Valley Drive, Mail Stop 926A, Reston, VA 20192. [2]Department of Earth, Atmospheric, and Planetary Sciences, Purdue University, West Lafayette, IN 47907. [3]Department of Geosciences and Don Sundquist Center of Excellence in Paleontology, East Tennessee State University, Johnson City, TN 37614. [*]Corresponding author - wodom@usgs.gov.

Associate Editor: Blaine Schubert, East Tennessee State University.

Background

Sinkhole complex formation and filling

The GFS sinkhole complex lies within Cambrian–Ordovician dolomite of the karst landscape that dominates the Tennessee Valley and Ridge Province (Fig. 1; Rodgers 1953). Gravimetric surveying by Whitelaw et al. (2008) revealed that the site consists of multiple sinkholes with depths up to ~35 m. The semi-linear trend of these sinkholes likely reflects joint-related dissolution. Though the formation age of the sinkhole complex itself is difficult to constrain, its filling with sediments and fossils during the late Cenozoic has been intensively studied. Shunk et al. (2006, 2009) examined the stratigraphy of cores (GFS-1 and GFS-2) through the sinkhole complex and interpreted the site as a filled sinkhole lake on the basis of excellent depositional fabric preservation, a lack of bioturbation, and presence of framboidal pyrite. The frequency of articulated skeletons over much of the site also suggests a predominantly low energy lacustrine environment (Hulbert et al. 2009, Wallace 2004, Wallace and Wang 2004). Shunk et al. (2006, 2009) also noted centimeter-scale graded beds overlain by rhythmites in the lower sinkhole complex, which the authors interpreted as a transition to a wetter period. Keenan and Engel (2017) further supported the low energy interpretation, noting that the sediments were likely acidic, anoxic, and reducing when deposited.

Sediments filling the sinkhole complex appear to be from multiple sources (Shunk et al. 2006, 2009). Grain size distributions of quartz within GFS-1 and estimates from flow velocity diagrams suggest that the core was located near the paleo-lake's inlet, and that low-energy fluvial transport was responsible for delivering sediments to the site (Shunk et al. 2009). This conclusion is supported by a general westward coarsening of sediments, indicating that most sediment flux was from the sinkhole complex's western side. Shunk et al.

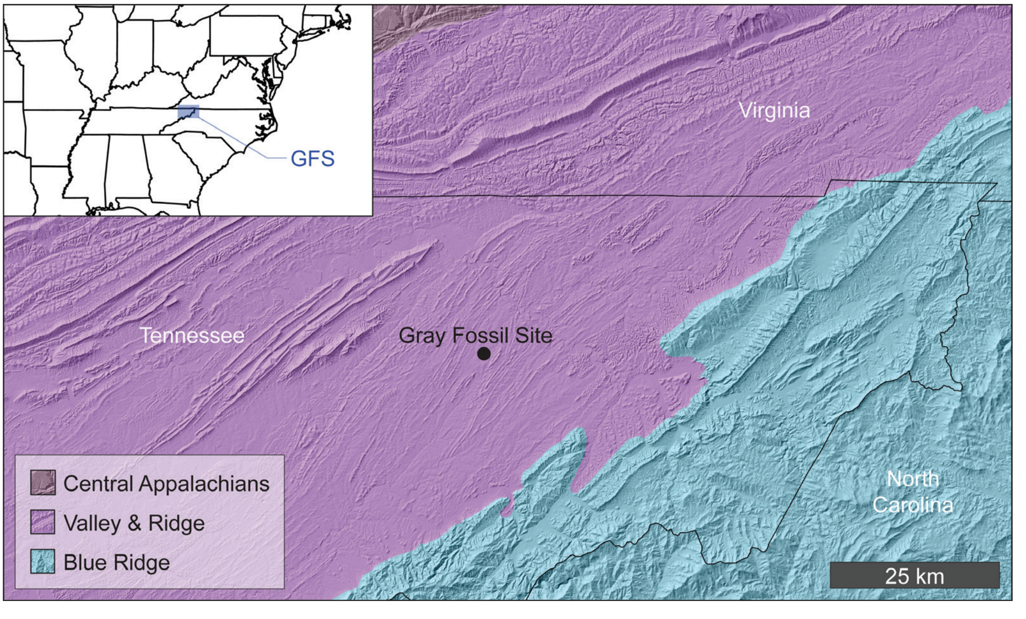

Figure 1. Location of the Gray Fossil Site in the context of major physiographic provinces of the southern Appalachian Mountains. A Blue Ridge provenance has been inferred for the sediments filling the Gray Fossil Site sinkhole complex (Shunk et al. 2006). Province polygons adapted from U.S. Environmental Protection Agency (2013).

(2006) also noted that some quartz grains had features consistent with Blue Ridge Province provenance (namely beta outlines, embayments, and resorption rims) that point to local and regional sources for the sediments filling the GFS basin.

Biostratigraphy

While the lacustrine depositional setting and Blue Ridge Province sediment provenance of the GFS fill have been generally accepted, the timing of its filling has been revised with emerging biostratigraphy (e.g., Samuels and Schap 2021, Samuels et al. 2018). Based on varve-like stratigraphy in GFS-1 and GFS-2, Shunk et al. (2009) estimated that the sinkhole complex filled geologically quickly over a period of 4.5–11 kyr. During infilling, a diverse biota died and was preserved in the upper layers of the sinkhole complex (Shunk et al. 2006). Ongoing discoveries of vertebrates with independently constrained emergence/extinction timelines have permitted increasingly precise age estimates for the site. Wallace and Wang (2004) produced one of the first age estimates, suggesting a broad age of 7–4.5 Ma based on the presence of *Teleoceras* (Rhinoceros) and *Plionarctos* (Short-faced Bear). Subsequent changes in the accepted boundary of the Hemphillian Land Mammal age (Behrensmeyer and Turner 2013, Tedford et al. 2004), potential extensions of the range of *Teleoceras* (Farlow et al. 2001, Gustafson 2012, Madden and Dahlquest 1990, Martin 2021), and issues surrounding the records of *Plionarctos* (B. Schubert, Eastern Tennessee State University, Johnson City, TN, 2024, pers. comm.) draw attention to the limitations of only using a few taxa to constrain the age.

Palynological analysis by Zobaa et al. (2011) focused on the GFS-1 core. The authors provided significantly older estimates, concluding based on fossil palynomorphs that most of the sinkhole complex was deposited in the Paleocene–Eocene and subsequently covered with Miocene and younger sediments. This Paleocene–Eocene age was estimated from the early Cenozoic pollens *Caryapollenites imparalis*, *Caryapollenites inelegans*, and *Caryapollenites prodromus*. Zobaa et al. (2011) also inferred that the lack of Neogene grass pollen *Poaceae* could be consistent with a Paleocene–Eocene age, though it should be noted that some late Cenozoic pollen (*Cupuliferoipollenites pusillus, Tricolporopollenites kruschii, Ulmipollenites undulosus, Caryapollenites simplex, Tubulifloridites antipodica, Pinuspollenites strobipites, Malvacearumpollis mannanensis, Fraxinus Columbiana, Chenopodipollis granulata,* and *Pseudoschizaea ozeanica*) were also present. A closer look at the taxa present in their sample suggests that the interpretation of a truly Eocene age is not necessary to account for their observations.

Most recently, a Pliocene age of the sinkhole complex was proposed by Samuels et al. (2018) on the basis of rhinoceros, leporid, and cricetid remnants. Leporid and cricetid fossils provide a maximum estimated age and date to the onset of the Blancan North American Land Mammal Age (4.9 Ma). Samuels et al. (2018) infer a minimum age of 4.5 Ma from the presence of the rhinoceros *Teleoceras*, but they note that Gustafson (2012) documented *Teleoceras* as young as 3.5 Ma in North America. One potential issue is that biostratigraphic reference sites do not all have radiometric and/or paleomagnetic age constraints (Carrasco et al. 2005; references therein). In many cases, the reference fauna have been dated via stratigraphic or biostratigraphic correlation, rather than absolute techniques. More importantly, considering that most of these sites are located in western North America, the distances from reference fossil sites to the GFS leave open the possibility that the fauna at Gray did not live contemporaneously with their western counterparts. As such, considerable uncertainty still surrounds the age of the deposit and motivates direct radiometric dating of the site itself.

Materials and Methods

Cosmogenic nuclide production and systematics

Cosmogenic nuclides are rare isotopes that are produced when high-energy cosmic radiation interacts with the atmosphere, initiating a chain of spallation reactions that break apart nuclei to produce new isotopes. These reactions cascade through the atmosphere to below the ground surface and are responsible for producing multiple types of cosmogenic nuclides, which include meteoric (a.k.a., "garden variety"), as well as *in-situ* isotopes (Lal 1988, Nishiizumi et al. 1986). The former, including ^{14}C and ^{10}Be, are produced in the atmosphere and are present in organic materials and rainwater (Arnold and Libby 1949, Lal 1988), whereas the latter, such as ^{26}Al and ^{10}Be, are produced in rock at a rate on the order of 10^1–10^3 atoms per gram per year (Nishiizumi et al. 1989), and are therefore generally present in extremely low concentrations. Given that ^{26}Al and ^{10}Be are radioactive, and their production is sensitive to depth below the ground surface, they can serve as valuable indicators of weathering processes, water movement, rock exposure, and sediment burial (Granger et al. 1997, Lal and Arnold 1985, Morris 1991).

Meteoric cosmogenic nuclides

Meteoric ^{10}Be ($^{10}Be_{met}$) is generally produced by spallation of atmospheric N and O (Lal and Peters 1967) and, upon reaching the Earth's surface, mixes with ^9Be liberated via rock weathering processes (von Blanckenburg et al. 2012). At the surface, Be adsorbs onto soils as a function of acidity (Brown et al. 1992), so the $^{10}Be_{met}/^9Be$ ratio records information about environmental and weathering regimes (Graly et al. 2011, 2018; Singleton 2021; Singleton et al. 2017). Because much of the $^{10}Be_{met}$ is retained in the upper part of the soil, but ^9Be is released over a deeper weathering range, the $^{10}Be_{met}/^9Be$ ratio varies with depth (Maher and von Blanckenburg 2016). Flora also incorporate beryllium as they uptake nutrients from soil (Moore et al. 2021) and have a $^{10}Be_{met}/^9Be$ ratio that is similar to the average $^{10}Be_{met}/^9Be$ ratio in soil over their rooting depth. Because $^{10}Be_{met}$ is radioactive, with a meanlife of 2.005 ± 0.020 My (Chmeleff et al. 2010, Korschinek et al. 2010), it can be used for dating over a range of up to ~8 My, given that the initial $^{10}Be_{met}$ value can be reasonably constrained, following equation (1):

$$t = \tau_{10} \ln \left[\frac{\left(\frac{^{10}Be_{met}}{^{9}Be} \right)_{initial}}{\left(\frac{^{10}Be_{met}}{^{9}Be} \right)_{final}} \right]$$

Where t is age and τ_{10} is the meanlife of ^{10}Be. This approach was originally used for dating marine deposits such as ferromanganese nodules (e.g., Graham et al. 2004, Somayajulu 1967), assuming that the $^{10}Be_{met}/^9Be$ ratio in seawater was constant over time. Later, these same data were used together with independent geochronometers to test the hypothesis that the $^{10}Be_{met}/^9Be$ ratio in seawater was constant, and have been used to infer that global weathering rates have remained approximately unchanged over the past 10 My (Willenbring and von Blanckenburg 2010). The $^{10}Be_{met}/^9Be$ ratio has also been used to date authigenic minerals in lake deposits, assuming that the lake water $^{10}Be_{met}/^9Be$ ratio was constant over time, notably to date Miocene–Pliocene hominid-bearing deposits in Chad (Lebatard et al. 2010).

Here, we are using $^{10}Be_{met}/^9Be$ to date soil sediments and vegetation that were deposited in the GFS sinkhole complex and extracted from the lower GFS-1 core. Unlike marine or lacustrine settings, the beryllium comes from a soil reservoir that includes significant variability in the initial isotopic ratio, introducing uncertainty (Graham et al. 2001, Moore et al. 2021). Additional uncertainty arises because the fallout rate of ^{10}Be varies through time due to changes in the geomagnetic field strength, as well as local or regional changes in precipitation (von Blanckenburg et al. 2012), the latter of which has been modeled for GFS (Schap et al. 2021).

***In-situ* cosmogenic nuclides**

In-situ ^{26}Al and ^{10}Be are produced when incoming neutrons and muons respectively fragment the Si and O in quartz (Gosse and Phillips 2001). Cosmogenic nuclide production is highest near the surface and falls off rapidly with depth, as cosmic radiation is attenuated by sediments and/or bedrock (Lal 1988). Production of cosmogenic nuclides by neutrons is limited to the top few meters near the ground surface, while slower production by muons continues to depths of tens of meters (Balco 2017). To a close approximation, the production rate P_i for a given nuclide *i* can be expressed as the sum of exponentials, as in equation (2):

$$P_i(z) = \sum_j A_{i,j} e^{-z/L_j}$$

Where $A_{i,j}$ and L_j represent the production rate factors and penetration length factors for neutron and muon components of production, respectively, and z represents depth (Granger 2014). For an eroding landscape, equation (2) can be integrated to calculate the concentration of cosmogenic nuclides that accumulate in a rock as it is exhumed to the surface (Lal 1991). For a steady rate of mass loss, the concentration N_i is inversely proportional to the denudation rate at the ground surface, with adjustments for radioactive decay during exhumation (Lal 1991), as in equation (3):

$$N_i(z) = \sum_j \frac{A_{i,j} e^{-z/L_j}}{\frac{1}{\tau_i} + \frac{\rho E}{\Lambda}}$$

Where ρ is the density of quartz, E is the preburial erosion rate, and Λ is the penetration length factor. If sediment from the ground surface is then buried underground, such as at GFS, any ^{26}Al and ^{10}Be that accumulated prior to deposition will begin to decay. Because ^{26}Al ($\tau_{26} = 1.021 \pm 0.024$ My) (Nishiizumi 2004) decays approximately twice as fast as ^{10}Be, the ^{26}Al/^{10}Be ratio of the cosmogenic nuclides inherited from the surface decreases over time and can be used to determine the time of deposition. However, there can be continued cosmogenic nuclide accumulation if the sediment is not buried deeply enough to be shielded from secondary cosmic ray muons. In that case, the total cosmogenic nuclide concentration N_i is governed by both radioactive decay of the inherited component and buildup of the post-depositional component, as in equation (4):

$$N_i(z,t) = e^{-t/\tau_i} \sum_j \frac{A_{i,j} e^{-z/L_j}}{\frac{1}{\tau_i} + \frac{\rho E}{\Lambda}} + P_{i,z}\tau_i\left(1 - e^{-t/\tau_i}\right)$$

Where t is the burial age and $P_{i,z}$ is the production rate at depth. The age of the deposit can be calculated by solving equation (4) for both ^{26}Al and ^{10}Be in a depth profile (Granger and Smith 2000) or in an isochron (Balco and Rovey 2008). In cases where the production rate at depth cannot be reliably modeled, it can be assumed to be zero to calculate a *minimum* burial age at each sampled location. Given the difficulty in modeling postburial production rates at this site, we calculated all *in-situ* burial ages as minima by setting $P_{26,z} = P_{10,z} = 0$ at/g/yr.

Both the *in-situ* and meteoric cosmogenic nuclide methods offer distinct advantages and disadvantages. Meteoric ^{10}Be/^{9}Be is typically present in relatively high concentrations in soils and plants and is, therefore, easy to measure. Moreover, the 2.005 My meanlife of ^{10}Be may permit geochronology well into the late Miocene. However, constraining the initial ratio of $^{10}Be_{met}/^{9}Be$ in a deposit can be difficult (Lebatard et al. 2010), and geochronologists may be limited to using $^{10}Be_{met}/^{9}Be$ in modern soils or plants, which are not a perfect analog. For *in-situ* cosmogenic ^{26}Al and ^{10}Be, estimating the initial component – in this case, the inherited ratio of $^{26}Al/^{10}Be$ in a buried deposit – is more straightforward (Granger et al. 1997). However, the shorter half-life of ^{26}Al means that $^{26}Al/^{10}Be$ burial dating is limited to the past 5–6 million years. Moreover, precise $^{26}Al/^{10}Be$ burial dating requires constraints on postburial production rates; while these rates can be readily modeled in homogeneous materials (Balco 2017), the irregular geometry of the sinkhole complex and variations in fill vs. bedrock density limit our ability to place upper constraints on sediment burial ages. We leverage the advantages of both approaches by measuring $^{10}Be_{met}/^{9}Be$ from the base of the GFS-1 core and *in-situ* $^{26}Al/^{10}Be$ in quartz at 8 intervals within the GFS-1 core to respectively obtain an absolute burial age for the basal sediments and 8 minimum burial ages throughout the core.

Sampling

Sediment samples for $^{10}Be_{met}/^{9}Be$ and *in-situ* $^{26}Al/^{10}Be$ geochronology were collected from the GFS-1 core at depths spanning 0.8 to 36.3 m. Core access was provided by the Gray Fossil Site and Museum, East Tennessee State University. Meteoric sampling focused on the base of the core to capture the age of the oldest sediments, while the $^{26}Al/^{10}Be$ depth profile covered the length of the core. Because the greatest change in the *in-situ* production rate occurs in the upper few meters of sediment column, as production transitions from neutron- to muon-dominated spallation, we sampled shallow zones at closer intervals for $^{26}Al/^{10}Be$ analysis. To constrain local initial $^{10}Be_{met}/^{9}Be$ ratios, we sampled modern grasses in undisturbed soils near Gray, Tennessee. All subsequent mineral separation, sample preparation, and analyses were performed at Purdue University.

$^{10}Be_{met}/^{9}Be$ sample preparation

A sample of material from the base of the GFS-1 core at a depth of 36.2–36.3 m was analyzed for $^{10}Be_{met}/^{9}Be$. The sample was extremely rich in organic material and plant fragments, which likely hosted much of the beryllium. 2.158 grams of oven-dried material were added to 25 ml of 0.5 M HCl. It was disaggregated by ultrasonication and held at 80°C for 24 hours to dissolve adsorbed beryllium, then the solution was filtered of solids.

A sample of grass clippings collected from the Gray, TN cemetery was used as an analog for the initial plant material in the GFS core. This site was chosen because it appeared undisturbed, so the $^{10}Be_{met}/^{9}Be$ ratio in vegetation should best represent the value prior to modern land use. Oven-dried grass (19 grams) was digested in piranha solution (sulfuric acid with hydrogen peroxide). After digestion, hydrofluoric acid was added to dissolve silica phytoliths. The resulting solution was taken to dryness, then redissolved in 5% nitric acid and filtered of insoluble residue.

For both the basal core and modern grass samples, half of the solution was taken for analysis of the total beryllium concentration by inductively coupled plasma – optical emission spectrometry (ICP-OES), and the other half was taken for analysis of $^{10}Be_{met}/^{9}Be$ by accelerator mass spectrometry (AMS). The AMS fraction was spiked with ~270 micrograms of beryllium carrier prepared in-house from phenacite. The solution was adjusted to pH 14 with NaOH to remove most contaminants as insoluble hydroxides by centrifugation, while amphoteric beryllium remained in solution. Beryllium was purified by ion exchange chromatography and selective precipitation, then converted to oxide by flame. The resulting oxide was mixed with niobium and loaded into a stainless-steel cathode for analysis by AMS at the Purdue Rare Isotope Measurement (PRIME) Laboratory.

In-situ **$^{26}Al/^{10}Be$ sample preparation**

Due to the compaction of the core material, high clay content, and small sample sizes, the samples required disaggregation prior to quartz separation. Samples were soaked overnight in concentrated nitric acid, rinsed, and mixed with sodium hexametaphosphate to disaggregate clays. Particularly cohesive materials were placed in an ultrasonic bath to disaggregate blocks of clay and sand. Grains with diameters >0.5 mm were removed via sieve to eliminate most chert and carbonate fragments. Samples that contained abundant chert and carbonate material underwent pyrophosphoric acid treatment following the methods of Mifsud et al. (2013) to preferentially attack non-quartz minerals. All samples were selectively dissolved in heated 1% hydrofluoric/nitric acid for 3 days on hot dog rollers to isolate the quartz fraction, and were assayed with ICP-OES.

Each sample received ~270 µg of beryllium carrier, and those with <1 mg native aluminum content additionally received an Alfa Aesar ICP aluminum standard as carrier. Samples were subsequently dissolved in hot concentrated hydrofluoric and nitric acids. Following extraction of an ICP-OES aliquot for total (native + carrier) aluminum content, the samples were evaporated with concentrated sulfuric acid. The resultant solution was diluted, mixed with 20 ml of 17% sodium hydroxide to remove Fe/Ti hydroxides at pH 14, and rinsed. Following dissolution in oxalic acid, the Al/Be solution was separated via anion and cation exchange column chromatography. The Al and Be were then respectively dissolved in hydrochloric and nitric acids, evaporated, and converted to oxides via propane torch. The resulting powders were mixed with niobium and loaded into stainless steel cathodes for AMS measurement at the PRIME Laboratory (Caffee et al. 2021). Measurements were conducted alongside the standards of Nishiizumi (2004) and Nishiizumi et al. (2007).

Results

Meteoric $^{10}Be/^{9}Be$

In modern local grass, the ^{10}Be concentration was $(2.133 \pm 0.037) \cdot 10^{7}$ at/g (1σ), and the ^{9}Be concentration was $1.025 \cdot 10^{15}$ at/g, yielding an initial $^{10}Be_{met}/^{9}Be$ ratio of $(208.18 \pm 3.64) \cdot 10^{-10}$ (1σ). Measurements of the core sample, in contrast, revealed $(9.139 \pm 0.088) \cdot 10^{7}$ at/g of ^{10}Be and $1.27 \cdot 10^{17}$ at/g of ^{9}Be, corresponding to a $^{10}Be_{met}/^{9}Be$ ratio of $(7.20 \pm 0.07) \cdot 10^{-10}$ (1σ) (Table 1). Taken together, these measurements provide an age of 6.74 ± 0.04 Ma (1σ) for the core's basal sediments, when accounting for analytical uncertainty only (Table 2).

Many factors contribute additional uncertainty. The fallout rate of ^{10}Be at a site can vary due to changes in the magnetic field and precipitation rate over time; evidence for the latter has been noted by Schap et al. (2021) for North America as a whole. However, data from DeSantis and Wallace (2008) show that the precipitation around Gray at the time of its infilling was very similar to that of the region's modern precipitation. The $^{10}Be_{met}/^{9}Be$ ratio in the soil depends on the weathering rate, which can change over time, as well as on soil depth. As a consequence, $^{10}Be_{met}/^{9}Be$ in modern vegetation can vary by 30% at a single site due to different rooting depths (e.g., Moore et al. 2021). Work by Graham et al. (2001) has demonstrated that $^{10}Be_{met}/^{9}Be$ in terrestrial materials (paleosols and loesses) from a given location can vary by ~5% over time. Given these possible variations, we assign a 35% uncertainty in the initial ratio. This assignment provides a less precise age of 6.60 ± 0.85 Ma (1σ) for the core's basal sediments (Fig. 2 and Table 2). As such, the $^{10}Be_{met}/^{9}Be$ data support a late Miocene age for initial sedimentation in the GFS-1 sinkhole.

Table 1. Chemical data and AMS results of meteoric $^{10}Be/^{9}Be$ samples. Analyses of $^{10}Be/^{9}Be$ were normalized to standard 07KNSTD ($2.85 \bullet 10^{-12}$) (Nishiizumi 2007). Reported values are blank-corrected. All uncertainties are reported at the 1σ level. Gray Grass was blank-corrected against Cblk 5559-1 [AMS Cathode # 167134, $^{10}Be/^{9}Be = (0.00 \pm 0.18) \cdot 10^{-15}$], while ETSU 2021-10 was blank-corrected against NRC blank [AMS Cathode # 165329, $^{10}Be/^{9}Be = (6.64 \pm 1.19) \cdot 10^{-15}$].

	Gray Grass	**ETSU 2021-10**
AMS cathode #	167117	163900
Sample mass (g)	19.040	2.158
Dissolved mass (g)	20.758	19.259
ICP-OES aliquot mass (g)	10.448	9.961
AMS aliquot mass (g)	10.310	9.298
Native ^{9}Be (µg)	0.147	2.118
^{9}Be carrier (µg)	293.581	293.382
$^{10}Be/^{9}Be$ (10^{-15})	10,280 ± 180	4864 ± 46
Blank-corrected $^{10}Be/^{9}Be$ (10^{-15})	10,280 ± 180	4857 ± 47
[^{9}Be] (10^{15} at/g)	1.025	127.000
[$^{10}Be_{met}$] (10^{7} at/g)	2.133 ± 0.037	9.139 ± 0.088
$^{10}Be_{met}/^{9}Be$ (10^{-10})	208.18 ± 3.64	7.20 ± 0.07

In-situ ^{26}Al/^{10}Be

Concentrations of ^{26}Al ranged from (0.3630 ± 0.0550) $\cdot 10^5$ at/g (1σ) (GF-49A) to (2.6070 ± 0.1760) $\cdot 10^5$ at/g (1σ) (GF-2A) (Table 3A), while ^{10}Be concentrations ranged from (0.4270 ± 0.0500) $\cdot 10^5$ at/g (1σ) (GF-35A) to (0.7270 ± 0.0510) $\cdot 10^5$ at/g (1σ) (GF-2A) (Table 3B). Blank corrections were generally low, although not negligible, ranging from 0.3–3.5% for ^{26}Al measurements and 2.0–9.9% for ^{10}Be measurements. The deepest sample (GF-49A), had ^{26}Al and ^{10}Be blank corrections of 3.2% and 2.3%, respectively. The

Table 2. Calculated meteoric ^{10}Be/^{9}Be ages for analytical and external uncertainties. Analytical uncertainties pertain to initial and final $^{10}Be_{met}/^{9}Be$ measurements, while external uncertainties only pertain to estimates of initial $^{10}Be_{met}/^{9}Be$. All ages and uncertainties that incorporate external uncertainties also incorporate analytical uncertainties. These ages correspond to the sediments at 36.2–36.3 m.

Mean age ± 1σ uncertainty (Ma)	**Uncertainty type**
6.74 ± 0.04	Analytical
6.74 ± 0.10	5% initial $^{10}Be_{met}/^{9}Be$ (Graham et al. 2001)
6.63 ± 0.69	30% local $^{10}Be_{met}/^{9}Be$ (Moore et al. 2021)
6.60 ± 0.85	35% total external uncertainty

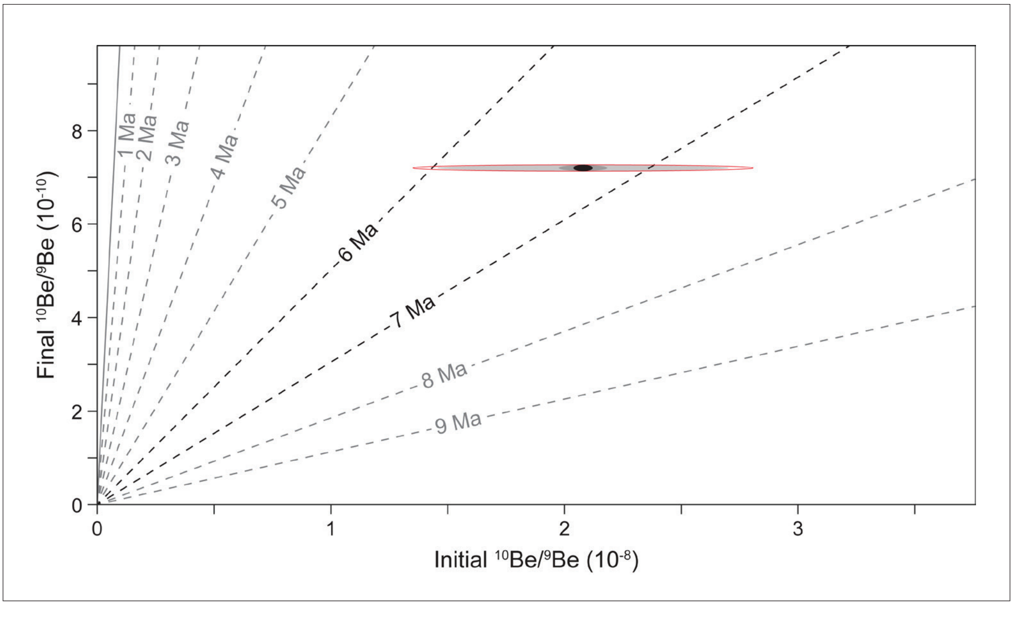

Figure 2. Age diagram for $^{10}Be_{met}/^{9}Be$ chronology. In this plot, the line corresponding to a zero burial age is solid. Isochron lines at million-year increments are dashed. Our measurements of initial and final $^{10}Be_{met}/^{9}Be$ are plotted with different potential uncertainties for initial $^{10}Be_{met}/^{9}Be$. A solid black ellipse shows analytical uncertainty only; gray ellipses show additional 5% uncertainty in continental $^{10}Be_{met}/^{9}Be$ following Graham et al. (2001) and 30% local variation in $^{10}Be_{met}/^{9}Be$ following Moore et al. (2021); a red outline shows the cumulative analytical and external uncertainties.

Table 3A. *In-situ* aluminum data for the GFS-1 core. All uncertainties are reported at the 1σ level. Analyses of $^{26}Al/^{27}Al$ were normalized to standard KNSTD ($1.818 \bullet 10^{-12}$) following Nishiizumi et al. (2004). NOTE: Depths are taken from top of core and do not reflect anthropogenic removal of material.

Sample name	**Quartz mass (g)**	**GFS-1 depth (m)**	**AMS cathode**	**Blank #**	**Total Al (μg)**	**$^{26}Al/^{27}Al$ (10^{-15})**	**^{26}Al (10^{6} at)**	**Corrected ^{26}Al (10^{6} at)**	**Corrected [^{26}Al] (10^{6} at/g)**
GF-2A	11.646	0.8	157516	14	1731	79.03 ± 4.88	3.0533 ± 0.1885	3.0366 ± 0.2044	0.2607 ± 0.0176
GF-5A	23.523	3.0	157517	14	3942	54.32 ± 3.27	4.7791 ± 0.2877	4.7625 ± 0.3036	0.2025 ± 0.0129
GF-8A	33.839	5.0	157518	14	8028	33.45 ± 2.46	5.9935 ± 0.4408	5.9769 ± 0.4567	0.1766 ± 0.0135
GF-10A	23.304	6.2	157519	14	3706	47.33 ± 3.12	3.9149 ± 0.2581	3.8983 ± 0.2740	0.1673 ± 0.0118
GF-19A	12.934	12.8	157520	14	1879	36.68 ± 3.16	1.5383 ± 0.1325	1.5217 ± 0.1484	0.1176 ± 0.0115
GF-26A	13.056	17.9	157521	14	2013	20.50 ± 2.11	0.9210 ± 0.0948	0.9044 ± 0.1107	0.0693 ± 0.0085
GF-35A	8.921	24.8	157522	14	1589	13.42 ± 2.01	0.4759 ± 0.0713	0.4593 ± 0.0872	0.0515 ± 0.0098
GF-49A	23.611	34.8	154879	11	2237	17.76 ± 2.30	0.8867 ± 0.1148	0.8580 ± 0.1307	0.0363 ± 0.0055
WO_BLK11	---	---	154885	---	1138	1.13 ± 1.30	0.0287 ± 0.0330	---	---
WO_BLK14	---	---	157523	---	1048	0.71 ± 0.68	0.0166 ± 0.0159	---	---

Table 3B. *In-situ* beryllium data for the GFS-1 core. All uncertainties are reported at the 1σ level. Analyses of $^{10}Be/^{9}Be$ were normalized to standard 07KNSTD ($2.85 \cdot 10^{-12}$) following Nishiizumi (2007). NOTE: Depths are taken from top of core and do not reflect anthropogenic removal of material.

Sample name	**Quartz mass (g)**	**GFS-1 depth (m)**	**AMS cathode**	**Blank #**	**Carrier Be (µg)**	**$^{10}Be/^{9}Be$ (10^{-15})**	**^{10}Be (10^{6} at)**	**Corrected ^{10}Be (10^{6} at)**	**Corrected [^{10}Be] (10^{6} at/g)**
GF-2A	11.646	0.8	157500	14	261.9	50.73 ± 2.79	0.8878 ± 0.0488	0.8461 ± 0.0589	0.0727 ± 0.0051
GF-5A	23.523	3.0	157501	14	260.0	91.30 ± 2.98	1.5862 ± 0.0518	1.5445 ± 0.0618	0.0657 ± 0.0026
GF-8A	33.839	5.0	157502	14	270.8	116.66 ± 4.05	2.1110 ± 0.0733	2.0693 ± 0.0833	0.0612 ± 0.0025
GF-10A	23.304	6.2	157503	14	261.4	82.53 ± 4.26	1.4415 ± 0.0744	1.3999 ± 0.0845	0.0601 ± 0.0036
GF-19A	12.934	12.8	157504	14	270.0	39.70 ± 2.37	0.7163 ± 0.0428	0.6746 ± 0.0528	0.0522 ± 0.0041
GF-26A	13.056	17.9	157505	14	269.0	37.07 ± 2.02	0.6663 ± 0.0363	0.6247 ± 0.0464	0.0478 ± 0.0036
GF-35A	8.921	24.8	157506	14	269.0	23.52 ± 1.90	0.4228 ± 0.0342	0.3811 ± 0.0442	0.0427 ± 0.0050
GF-49A	23.611	34.8	154871	11	266.2	61.69 ± 3.21	1.0973 ± 0.0571	1.0719 ± 0.0687	0.0454 ± 0.0029
WO_ BLK11	---	---	184877	---	266.3	1.43 ± 0.65	0.0254 ± 0.0116	---	---
WO_ BLK14	---	---	157507	---	268.8	2.32 ± 0.56	0.0417 ± 0.0101	---	---

^{10}Be and ^{26}Al concentrations showed exponential relationships with depth (Fig. 3). Attempts to model the postburial production of ^{26}Al and ^{10}Be to obtain an absolute burial age for the GFS-1 core sediments were stymied by (a) poor constraints on the cosmic ray flux throughout the sinkhole complex, which is influenced by the complicated geometry of surrounding bedrock, and (b) low concentrations of inherited cosmogenic ^{26}Al and ^{10}Be (Odom 2020). As such, here we report only *minimum* burial ages derived from *in-situ* cosmogenic ^{26}Al and ^{10}Be. Minimum burial age calculations for each sample depth (which are calculated assuming no postburial production of ^{26}Al or ^{10}Be) are provided in Figure 3 and Table 4, and ranged from 1.32 ± 0.20 Ma (1σ) at the shallowest sample location to 4.43 ± 0.34 Ma (1σ)

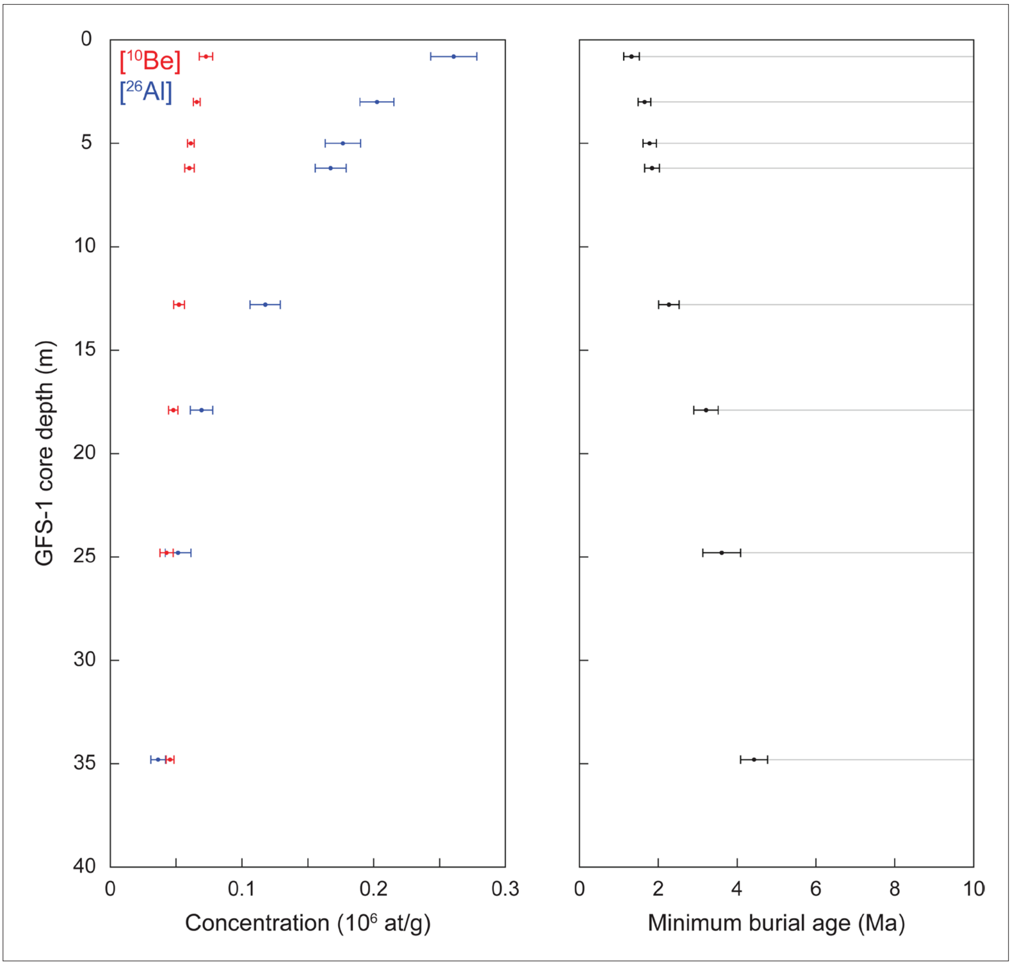

Figure 3. *In-situ* cosmogenic nuclide concentrations and minimum burial age data throughout the GFS-1 core. Depths are listed from the top of the GFS-1 core, which was bored in an excavated area; as such, the listed depths are several meters shallower than they would have been for much of the deposit's existence. Left: Concentrations of ^{26}Al and ^{10}Be with depth in the GFS-1 core. All uncertainties shown are at the 1σ level. Right: Minimum burial ages (assuming no postburial production) of the *in-situ* samples from the GFS-1 core. Gray lines extend from the mean ± 1σ minimum burial ages to emphasize that these ages are only minimum bounds on the burial ages of the GFS-1 sediments. The infeasibility of modeling postburial production at this location precludes this study from placing maximum bounds on any of the ^{26}Al/^{10}Be burial ages.

Table 4. Measured $^{26}Al/^{10}Be$ ratios and minimum burial ages (assuming zero post-burial production of ^{26}Al or ^{10}Be) for *in-situ* samples in the GFS-1 core. All uncertainties are reported at the 1σ level. Given the poorly constrained geometry of the sinkhole complex, estimates of postburial production rates and relevant maximum burial ages have not been included due to the poor age constraints they provide (Odom 2020).

Sample name	**GFS-1 depth (m)**	**Corrected $^{26}Al/^{10}Be$**	**Minimum burial age (Ma)**
GF-2A	0.8	3.59 ± 0.35	1.32 ± 0.20
GF-5A	3.0	3.08 ± 0.23	1.65 ± 0.16
GF-8A	5.0	2.89 ± 0.25	1.78 ± 0.17
GF-10A	6.2	2.78 ± 0.26	1.84 ± 0.19
GF-19A	12.8	2.25 ± 0.28	2.27 ± 0.26
GF-26A	17.9	1.45 ± 0.21	3.21 ± 0.31
GF-35A	24.8	1.21 ± 0.27	3.61 ± 0.48
GF-49A	34.8	0.80 ± 0.13	4.43 ± 0.34

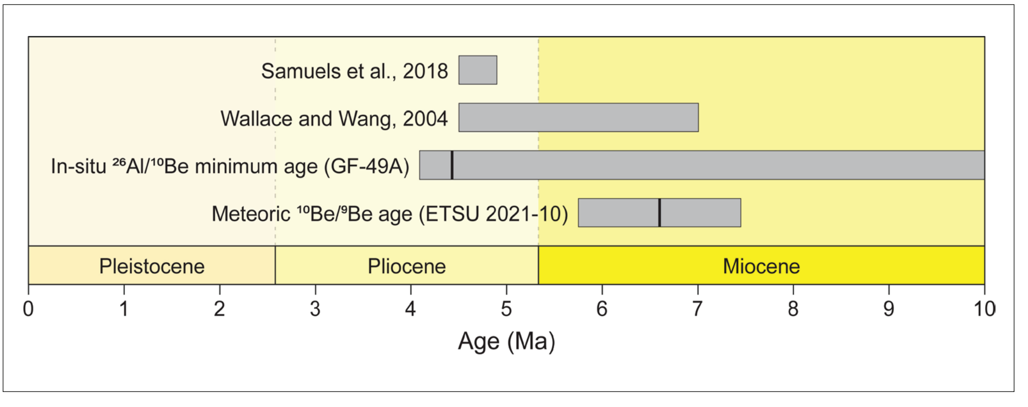

Figure 4. Results of $^{26}Al/^{10}Be$ and meteoric $^{10}Be/^{9}Be$ geochronology in the context of previous age estimates (Samuels et al., 2018, Wallace and Wang 2004) and the geologic timescale. Mean values are shown as black vertical lines and boxes are shaded to include ± 1σ uncertainties for cosmogenic nuclide ages. The oldest $^{26}Al/^{10}Be$ minimum burial age (4.43 ± 0.34 Ma), derived from the deepest *in-situ* sample at 34.8 meters below core top, is shown. The sample from which this minimum burial age was derived experienced the least postburial production of ^{26}Al and ^{10}Be out of all the *in-situ* samples, and therefore should yield the most realistic minimum burial age. Its range of possible ages extends to infinity, as a maximum age cannot be modeled. The meteoric $^{10}Be/^{9}Be$ age (6.60 ± 0.85 Ma), derived from sample ETSU 2021-10, is plotted with 35% total external uncertainty.

at the deepest sample location. This increase in minimum age with depth likely reflects decreasing postburial production, and neither necessitates nor excludes an upward-younging trend for the sediments. Based on ^{26}Al/^{10}Be data alone, however, it is clear that the burial of basal sediments at 34.8 m depth (sample GF-49A) dates to at least the early Pliocene and may have occurred earlier.

Discussion

Synthesizing meteoric ^{10}Be/^{9}Be and *in-situ* ^{26}Al/^{10}Be ages

The 2 cosmogenic nuclide geochronology techniques used in this study converge on a consistent burial age for the basal sediments in the GFS-1 core (Fig. 4). Deposition of the basal sediments is well constrained by the meteoric ^{10}Be/^{9}Be age of 6.60 ± 0.85 Ma, which represents an absolute age (i.e., one with younger and older bounds) for sediments at 36.2–36.3 m depth. With 1σ external uncertainty, this age falls entirely within the late Miocene. The *in-situ* geochronology provides a looser constraint on sediment ages, given that maximum boundaries cannot be placed on ^{26}Al/^{10}Be burial ages due to difficulty modeling the postburial production of ^{26}Al and ^{10}Be. While exact rates of postburial production could not be modeled, it is reasonable to infer that the deepest *in-situ* sample, GF-49A, was least affected and would, therefore, yield a minimum burial age closest to its true burial age. This minimum burial age, 4.43 ± 0.34 Ma, demonstrates that the sediments at 34.8 m depth were, indeed, at least early Pliocene in age. While this minimum age does overlap with recent biochronologic estimates for the uppermost GFS (Samuels et al. 2018), it is critical to note that this age is a minimum only, and that the maximum age remains unbounded to infinity. As such, it is also consistent with the meteoric ^{10}Be/^{9}Be age located less than 2 meters below it that places a late Miocene age on the basal sediments.

Revisiting an early Cenozoic age for the base of the GFS-1 core

Our data support a late Miocene age for the basal GFS-1 core sediments, contrasting with the observations of Zobaa et al. (2011) that estimated a Paleocene–Eocene age for the lower portion of the GFS-1 core. A re-examination of the palynological data presented in Zobaa et al. (2011) reveals the presence of several pollen types that were present during the late Cenozoic (*Cupuliferoipollenites pusillus, Tricolporopollenites kruschii, Ulmipollenites undulosus, Caryapollenites simplex, Tubulifloridites antipodica, Pinuspollenites strobipites, Malvacearumpollis mannanensis, Fraxinus Columbiana, Chenopodipollis granulata,* and *Pseudoschizaea ozeanica*) (White 2008 and references therein) that are consistent with our age finding. Zobaa et al. (2011) hypothesized that younger fossil pollen had percolated through cracks and fractures into the cored section, but it appears more likely that older pollen was preserved in the gradually eroding Cenozoic landscape and subsequently deposited in the sinkhole complex during the late Miocene.

Biostratigraphic considerations

Given that our data exclude a Paleocene–Eocene age and support a Neogene age for the lower sediments of the GFS-1 core, we consider the Neogene biostratigraphy that has thus far provided the most consistent age estimates for the uppermost sections of the deposit. The biostratigraphic age estimates for the Gray Fossil Site have generally corresponded to the late Miocene and early Pliocene. Using bear and rhinoceros fossils, Wallace and Wang (2004) estimated that the deposit dated to 7–4.5 Ma, which includes both the late Miocene and early Pliocene. The later works of Samuels et al. (2018), Bōgner and Samuels (2022), and Oberg and Samuels (2022) pointed to an early Pliocene age. Our most likely meteoric $^{10}Be/^{9}Be$ age indicates a late Miocene age for the basal sediments that underlie the fauna. It is possible that, if the sinkhole filled slowly or unconformities occurred in the sequence, the lower sediments could be late Miocene in age while the shallower sediments could date to the early Pliocene.

Alternatively, it is possible that sinkhole filling rapidly transpired over several thousand years during the late Miocene, as estimated by Shunk et al. (2009). In this case, perceived disagreements between faunal age estimates and cosmogenic nuclide geochronology could be tied to the current constraints on fauna used for biostratigraphy, as well as the sensitivity of the cosmogenic $^{26}Al/^{10}Be$ and $^{10}Be_{met}/^{9}Be$ techniques to the surrounding environment. It is also possible that the fossil record employed by biostratigraphers at the GFS has underestimated the dates of first appearance for *Alilepus vagus*, *Neotoma*, *Notolagus lepusculus*, and *Symmetrodontomys* fossils. Those taxa identified to the genus-level only could, in fact, represent new taxa, and those identified to species are far removed (geographically) from their closest counterparts. Given the existing data, however, it is not possible to determine the radiometric age of the fossil-bearing upper sinkhole deposits.

Conclusions

This study provides the first direct radiometric constraints on the age of the lower Gray Fossil Site deposit. Minimum burial ages derived from our $^{26}Al/^{10}Be$ measurements for the GFS-1 core strongly point to a minimum early Pliocene age, but cannot place definite upper bounds on the age of the sinkhole complex. This age estimate is further constrained by our $^{10}Be_{met}/^{9}Be$ age for the sinkhole complex's basal sediments (6.60 ± 0.85 Ma), which falls within the late Miocene. It is difficult to determine whether the entire GFS deposit – and the biota within – dates to only the late Miocene, or if the deposit youngs upward into the early Pliocene. If the entire deposit is late Miocene in age, the GFS could potentially represent a "first appearance" site or unique transitional ecosystem (something between the Hemphillian and Blancan). Further geochronology in the form of additional $^{10}Be_{met}/^{9}Be$ measurements or paleomagnetic analysis could provide additional constraints on the age of the upper GFS and the biota within.

Acknowledgments

This work was funded by National Science Foundation EAR1700821 to D.E. Granger. We thank Randall Orndorff, Nicholas Powell, Robert Stamm, and 2 anonymous reviewers for their recommendations that improved the quality of this manuscript. Any use of trade, firm, or product names is for descriptive purposes only and does not imply endorsement by the U.S. Government.

Literature Cited

Arnold, J.R., and W.F. Libby. 1949. Age determinations by radiocarbon content: Checks with samples of known age. Science 110(2869):678–680. https://doi.org/10.1126/science.110.2869.678

Balco, G. 2017. Production rate calculations for cosmic-ray-muon-produced ^{10}Be and ^{26}Al benchmarked against geological calibration data. Quaternary Geochronology 39:150–173. https://doi.org/10.1016/j.quageo.2017.02.001

Balco, G., and C.W. Rovey. 2008. An isochron method for cosmogenic-nuclide dating of buried soils and sediments. American Journal of Science 308(10):1083–1114. doi.org/10.2475/10.2008.02

Behrensmeyer, A.K., and A. Turner. 2013. Taxonomic occurrences of Suidae recorded in the Paleobiology Database. http://fossilworks.org

Boardman, G.S., and B.W. Schubert. 2011. First Mio-Pliocene salamander fossil assemblage from the southern Appalachians. Palaeontologia Electronica 14(2)16A:1–19. palaeo-electronica.org/2011_2/257/index.html

Bōgner, E., and J.X. Samuels. 2022. The first canid from the Gray Fossil Site in Tennessee: New perspective on the distribution and ecology of *Borophagus*. Journal of Paleontology 96(6):1379–1389. https://doi.org/10.1017/jpa.2022.46

Bourque, J.A., and B.W. Schubert. 2015. Fossil musk turtles (Kinosternidae, *Sternotherus*) from the late Miocene–early Pliocene (Hemphillian) of Tennessee and Florida. Journal of Vertebrate Paleontology e885441:1–19. http://dx.doi.org/10.1080/02724634.2014.885441

Brown, E.T., J.M. Edmond, G.M. Raisbeck, D.L. Bourles, F. Yiou, and C.I. Measures. 1992. Beryllium isotope geochemistry in tropical river basins. Geochimica et Cosmochimica Acta 56:1607–1624. https://doi.org/10.1016/0016-7037(92)90228-B

Caffee, M., N. Lifton, G. Chmiel, G. Jackson, L. Luo, P. Muzikar, T. Woodruff, and D. Granger. 2021. Accelerator Mass Spectrometry at Purdue University PRIME Lab. 15th International Conference on Accelerator Mass Spectrometry. Sydney, Australia.

Carrasco, M.A., B.P. Kraatz, E.B. Davis, and A.D. Barnosky. 2005. Miocene mammal mapping project (MIOMAP). https://ucmp.berkeley.edu/miomap/index-original.html

Chmeleff, J., F. von Blanckenburg, K. Kossert, and D. Jakob. 2010. Determination of the ^{10}Be half-life by multicollector ICP-MS and liquid scintillation counting. Nuclear Instruments and Methods in Physics Research Section B: Beam Interactions with Materials and Atoms 268:92–199. https://doi.org/10.1016/j.nimb.2009.09.012

Czaplewski, N.J. 2017. First report of bats (Mammalia: Chiroptera) from the Gray Fossil Site (late Miocene or early Pliocene), Tennessee, USA. PeerJ 5:e3263:1–18. https://doi.org/10.7717/peerj.3263

DeSantis, L.R., and S.C. Wallace. 2008. Neogene forests from the Appalachians of Tennessee, USA: Geochemical evidence from fossil mammal teeth. Palaeogeography, Palaeoclimatology, Palaeoecology 266(1-2):59–68. https://doi.org/10.1016/j.palaeo.2008.03.032

Doughty, E.M., S.C. Wallace, B.W. Schubert, and L.M. Lyon. 2018. First occurrence of the enigmatic peccaries *Mylohyus elmorei* and *Prosthennops serus* from the Appalachians: Latest Hemphillian to Early Blancan of Gray Fossil Site, Tennessee. PeerJ 6:e5926:1–31. http://doi.org/10.7717/peerj.5926

Farlow, J.O., J.A. Sunderman, J.J. Havens, A.L. Swinehart, J.A. Holman, R.L. Richards, N.G. Miller, R.A. Martin, R.M. Hunt Jr., G.G. Storrs, B.B. Curry, R.H. Fluegeman, M.R. Dawson, and M.E.T. Flint. 2001. The Pipe Creek Sinkhole biota, a diverse late Tertiary continental fossil assemblage from Grant County, Indiana. American Midland Naturalist 145:367–378. https://doi.org/10.1674/0003-0031(2001)145[0367:TPCSBA]2.0.CO;2

Fulwood, E.L., and S.C. Wallace. 2015. Evidence for unusual size dimorphism in a fossil ailurid. Palaeontologia Electronica 18(3)45A:1–6. palaeo-electronica.org/content/2015/1313-dimorphism-in-pristinailurus

Gong, F., I. Karsai, and Y.C. Liu. 2010. Vitis seeds (Vitaceae) from the late Neogene Gray Fossil Site, northeastern Tennessee, U.S.A. Review of Palaeobotany and Palynology 162:71–83. https://doi.org/10.1016/j.revpalbo.2010.05.005

Gosse, J., and F. Phillips. 2001. Terrestrial in situ cosmogenic nuclides: Theory and application. Quaternary Science Reviews 20(14):1475–1560. https://doi.org/10.1016/S0277-3791(00)00171-2

Graham, I.J., R.M. Carter, R.G. Ditchburn, and A. Zondervan. 2004. Chronostratigraphy of ODP 181, Site 1121 sediment core (Southwest Pacific Ocean), using ^{10}Be/^{9}Be dating of entrapped ferromanganese nodules. Marine Geology 205(1-4):227–247. https://doi.org/10.1016/S0025-3227(04)00025-8

Graham, I.J., R.G. Ditchburn, and N.E. Whitehead. 2001. Be isotope analysis of a 0–500 ka loess–paleosol sequence from Rangitatau East, New Zealand. Quaternary International 76:29–42. https://doi.org/10.1016/S1040-6182(00)00087-2

Graly, J.A., L.B. Corbett, P.R. Bierman, A. Lini, and T.A. Neumann. 2018. Meteoric ^{10}Be as a tracer of subglacial processes and interglacial surface exposure in Greenland. Quaternary Science Reviews 191:118–131. https://doi.org/10.1016/j.quascirev.2018.05.009

Graly, J.A., L.J. Reusser, and P.R. Bierman. 2011. Short and long-term delivery rates of meteoric ^{10}Be to terrestrial soils. Earth and Planetary Science Letters 302(3-4):329–336. https://doi.org/10.1016/j.epsl.2010.12.020

Granger, D.E. 2014. Cosmogenic nuclide burial dating in archaeology and paleoanthropology. Pp 81-97, *In* Cerling, T.E. (Ed.). Archaeology and Anthropology: Treatise on Geochemistry 12(8). Elsevier Pergamon, Oxford, UK. http://dx.doi.org/10.1016/B978-0-08-095975-7.01208-0

Granger, D.E., and A.L. Smith. 2000. Dating buried sediments using radioactive decay and muogenic production of ^{26}Al and ^{10}Be. Nuclear Instruments and Methods in Physics Research Section B: Beam Interactions with Materials and Atoms 172(1-4):822–826. https://doi.org/10.1016/S0168-583X(00)00087-2

Granger, D.E., J.W. Kirchner, and R.C. Finkel. 1997. Quaternary downcutting rate of the New River, Virginia, measured from differential decay of cosmogenic ^{26}Al and ^{10}Be in cave-deposited alluvium. Geology 25(2):107–110. https://doi.org/10.1130/0091-7613(1997)025%3C0107:QDROTN%3E2.3.CO;2

Gunnin, D., B.W. Schubert, J.X. Samuels, K.E. Bredehoeft, and S. Maden. 2025. A new plethodontid salamander from the Early Pliocene of northeastern Tennessee, U.S.A., and its bearing on desmognathan evolution. Historical Biology 1–25. https://doi.org/10.1080/08912963.2025.2501332

Gustafson, E.P. 2012. New records of rhinoceroses from the Ringold Formation of central Washington and the Hemphillian-Blancan boundary. Journal of Vertebrate Paleontology 32(3):727–731. https://doi.org/10.1080/02724634.2012.658481

Hermsen, E.J. 2021. Review of the Fossil Record of *Passiflora*, with a Description of New Seeds from the Pliocene Gray Fossil Site, Tennessee, USA. International Journal of Plant Sciences 182(6):533–550. https://doi.org/10.1086/714282

Hermsen, E.J. 2023. Pliocene seeds of *Passiflora* subgenus *Decaloba* (Gray Fossil Site, Tennessee) and the impact of the fossil record on understanding the diversification and biogeography of *Passiflora*. American Journal of Botany 110:e16137. https://doi.org/10.1002/ajb2.16137

Huang, Y., Y.C. Liu, and M. Zavada. 2014. New fossil fruits of *Carya* (Juglandaceae) from the latest Miocene to earliest Pliocene in Tennessee, eastern United States. Journal of Systematics and Evolution 52(4):508–520. https://doi.org/10.1111/jse.12085

Huang, Y., Y. Liu, J. Wen, and C. Quan. 2015. First fossil record of *Staphylea L.* (Staphyleaceae) from North America, and its biogeographic implications. Plant Systematics and Evolution 301:2203–2218. https://doi.org/10.1007/s00606-015-1224-z

Hulbert, R.C., S.C. Wallace, W.E. Klippel, and P.W. Parmalee. 2009. Cranial morphology and systematics of an extraordinary sample of the late Neogene dwarf tapir, *Tapirus polkensis* (Olsen). Journal of Paleontology 83(2):238–262. https://doi.org/10.1666/08-062.1

Jasinski, S.E. 2018. A new slider turtle (Testudines: Emydidae: Deirochelyinae: *Trachemys*) from the late Hemphillian (late Miocene/early Pliocene) of eastern Tennessee and the evolution of the deirochelyines. PeerJ 6:e4338:1–81. https://doi.org/10.7717/peerj.4338

Jasinski, S.E. 2022. A new species of *Chrysemys* (Emydidae: Deirochelyinae) from the latest Miocene-Early Pliocene of Tennessee, USA and its implications for the evolution of painted turtles. Zoological Journal of the Linnean Society 198(1):149–183. https://doi.org/10.1093/zoolinnean/zlac084

Jasinski, S.E., and D.A. Moscato, 2017. Late Hemphillian Colubrid Snakes (Serpentes, Colubridae) from the Gray Fossil Site of Northeastern Tennessee. Journal of Herpetology 51(2):245–257. https://doi.org/10.1670/16-020

Jiang, Y.L., and Y. Liu. 2008. A simple and convenient determination of perylene preserved in the Late Neogene wood from northeastern Tennessee using fluorescence spectroscopy. Organic Geochemistry 39:1462–1465. https://doi.org/10.1016/j.orggeochem.2008.06.006

Jurestovsky, D.J. 2021. Small Colubroids from the Late Hemphillian Gray Fossil Site of Northeastern Tennessee. Journal of Herpetology 55(4):422–431. https://doi.org/10.1670/21-008

Keenan, S.W., and A.S. Engel. 2017. Reconstructing diagenetic conditions of bone at the Gray Fossil Site, Tennessee, USA. Palaeogeography, Palaeoclimatology, Palaeoecology 471:48–57. https://doi.org/10.1016/j.palaeo.2017.01.037

Korschinek, G., A. Bergmaier, T. Faestermann, U.C. Gerstmann, K. Knie, G. Rugel, A. Wallner, A., I. Dillmann, G. Dollinger, C.L. Von Gostomski, and K. Kossert. 2010. A new value for the half-life of ^{10}Be by heavy-ion elastic recoil detection and liquid scintillation counting. Nuclear Instruments and Methods in Physics Research Section B: Beam Interactions with Materials and Atoms 268:187–191. https://doi.org/10.1016/j.nimb.2009.09.020

Lal, D. 1988. In situ-produced cosmogenic isotopes in terrestrial rocks. Annual Review of Earth and Planetary Sciences 16:355–388. https://doi.org/10.1146/annurev.ea.16.050188.002035

Lal, D. 1991. Cosmic ray labeling of erosion surfaces: In situ nuclide production rates and erosion models. Earth and Planetary Science Letters 104(2-4):424–439. https://doi.org/10.1016/0012-821X(91)90220-C

Lal, D., and J.R. Arnold. 1985. Tracing quartz through the environment. Proceedings of the Indian Academy of Sciences-Earth and Planetary Sciences 94:1–5. https://doi.org/10.1007/BF02863403

Lal, D., and B. Peters. 1967. Cosmic ray produced radioactivity on the Earth. Kosmische Strahlung II/Cosmic Rays II. Berlin, Heidelberg: Springer Berlin Heidelberg 551–612. https://doi.org/10.1007/978-3-642-46079-1_7

Lebatard, A., D. Bourles, R. Braucher, M. Arnold, P. Duringer, M. Jolivet, A. Moussa, P. Deschamps, C. Roquin, J. Carcaillet, M. Schuster, F. Lihoreau, A. Likius, H. Mackaye, P. Vignaud, and M. Brunet. 2010. Application of the authigenic ^{10}Be/^{9}Be dating method to continental sediments: Reconstruction of the Mio-Pleistocene sedimentary sequence in the early hominid fossiliferous areas of the northern Chad Basin. Earth and Planetary Science Letters 297(1-2):57–70. https://doi.org/10.1016/j.epsl.2010.06.003

Liu, Y.C., and F.M.B. Jacques. 2010. *Sinomenium macrocarpum* sp. nov. (Menispermaceae) from the Miocene–Pliocene transition of Gray, northeast Tennessee, USA. Review of Palaeobotany and Palynology 159:112–122. https://doi.org/10.1016/j.revpalbo.2009.11.005

Liu, Y., and C. Quan. 2019. Neogene oak diversity of southeast United States: Pollen evidence from the Gray Fossil Site. Grana 59(1):19–24. https://doi.org/10.1080/00173134.2019.1675753

Maclaren, J.A., R.C. Hulbert Jr., S.C. Wallace, and S. Nauwelaerts. 2018. A morphometric analysis of the forelimb in the genus *Tapirus* (Perissodactyla: Tapiridae) reveals influences of habitat, phylogeny and size through time and across geographical space. Zoological Journal of the Linnean Society 184:499–515. https://doi.org/10.1093/zoolinnean/zly019

Madden, C.T., and W.W. Dahlquest. 1990. The last rhinoceros in North America. Journal of Vertebrate Paleontology 10:266–267. https://doi.org/10.1080/02724634.1990.10011812

Maher, K., and F. von Blanckenburg. 2016. Surface ages and weathering rates from ^{10}Be (meteoric) and ^{10}Be/^{9}Be: Insights from differential mass balance and reactive transport modeling. Chemical Geology 446:70–86. https://doi.org/10.1016/j.chemgeo.2016.07.016

Martin, R.A. 2021. Correlation of Pliocene and Pleistocene fossil assemblages from the central and eastern United States: Toward a continental rodent biochronology, Historical Biology 33:6:880–896. https://doi.org/10.1080/08912963.2019.1666118

McConnell, S.M., and M.S. Zavada. 2013. The occurrence of an abdominal fauna in an articulated tapir (*Tapirus polkensis*) from the Late Miocene Gray Fossil Site, northeastern Tennessee. Integrative Zoology 8(1):74–83. https://doi.org/10.1111/j.1749-4877.2012.00320.x

Mead, J.M., B.W. Schubert, S.C. Wallace, and S.L. Swift. 2012. Helodermatid lizard from the Mio−Pliocene oak−hickory forest of Tennessee, eastern USA, and a review of monstersaurian osteoderms. Acta Palaeontologica Polonica 57(1):111–121. https://doi.org/10.4202/app.2010.0083

Mifsud, C., T. Fujioka, and D. Fink. 2013. Extraction and purification of quartz in rock using hot phosphoric acid for in situ cosmogenic exposure dating. Nuclear Instruments and Methods in Physics Research Section B: Beam Interactions with Materials and Atoms 294:203–207. https://doi.org/10.1016/j.nimb.2012.08.037

Moore, A.K., D.E. Granger, and G. Conyers. 2021. Beryllium cycling through deciduous trees and implications for meteoric ^{10}Be systematics. Chemical Geology 571:120174. https://doi.org/10.1016/j.chemgeo.2021.120174

Morris, J.D. 1991. Applications of ^{10}Be to problems in the earth sciences. Annual Review of Earth and Planetary Sciences 19:313. https://doi.org/10.1146/annurev.ea.19.050191.001525

Nishiizumi, K. 2004. Preparation of ^{26}Al AMS standards. Nuclear Instruments and Methods in Physics Research Section B: Beam Interactions with Materials and Atoms 223:388–392. https://doi.org/10.1016/j.nimb.2004.04.075

Nishiizumi, K., M. Imamura, M.W. Caffee, J.R. Southon, R.C. Finkel, and J. McAninch. 2007. Absolute calibration of ^{10}Be AMS standards. Nuclear Instruments and Methods in Physics Research Section B: Beam Interactions with Materials and Atoms 258:403–413. https://doi.org/10.1016/j.nimb.2007.01.297

Nishiizumi, K., D. Lal, J. Klein, R. Middleton, and J.R. Arnold. 1986. Production of ^{10}Be and ^{26}Al by cosmic rays in terrestrial quartz in situ and implications for erosion rates. Nature 319(6049):134–136. https://doi.org/10.1038/319134a0

Nishiizumi, K., E.L. Winterer, C.P. Kohl, J. Klein, R. Middleton, D. Lal, and J.R. Arnold. 1989. Cosmic ray production rates of ^{10}Be and ^{26}Al in quartz from glacially polished rocks. Journal of Geophysical Research: Solid Earth 94:B12:17907–17915. https://doi.org/10.1029/JB094iB12p17907

Oberg, D.E., and J.X. Samuels. 2022. Fossil moles from the Gray Fossil Site (Tennessee): Implications for diversification and evolution of North American Talpidae. Palaeontologia Electronica 25(3):a33. https://doi.org/10.26879/1150

Ochoa, D., M. Whitelaw, Y.S.C. Liu, and M. Zavada. 2012. Palynology of Neogene sediments at the Gray Fossil Site, Tennessee, USA: Floristic implications. Review of Palaeobotany and Palynology 184:36–48. https://doi.org/10.1016/j.revpalbo.2012.03.006

Odom, W.E. 2020. Dating the Cenozoic incision history of the Tennessee and Shenandoah Rivers with cosmogenic nuclides and ^{40}Ar/^{39}Ar in manganese oxides. PhD thesis. Purdue University. West Lafayette, Indiana, USA. 309 pp. https://doi.org/10.25394/PGS.13275017.v1

Parmalee, P.W., W.E. Klippel, P.A. Meylan, and J.A. Holman. 2002. A late Miocene-early Pliocene population of *Trachemys* (Testudines: Emydidae) from east Tennessee. Annals of Carnegie Museum 71(4):233–239.

Quirk, Z.J., and E.J. Hermsen. 2020. Neogene *Corylopsis* seeds from eastern Tennessee. Journal of Systematics and Evolution 59(3):611–621. https://doi.org/10.1111/jse.12571

Rodgers, J. 1953. Geologic map of east Tennessee with explanatory text. Bulletin 58, Tennessee Division of Geology.

Samuels, J.X., K.E. Bredehoeft, and S.C. Wallace. 2018. A new species of *Gulo* from the Early Pliocene Gray Fossil Site (Eastern United States); rethinking the evolution of wolverines. PeerJ 6:e4648:1–29. https://doi.org/10.7717/peerj.4648

Samuels, J.X., and J. Schap. 2021. Early Pliocene Leporids from the Gray Fossil Site of Tennessee. Eastern Paleontologist 8:1–23.

Schap, J.A., and J.X. Samuels. 2020. Mesowear Analysis of the *Tapirus polkensis* population from the Gray Fossil Site, Tennessee, USA. Palaeontologia Electronica 23(2):A26:1–16. https://doi.org/10.26879/875

Schap, J.A., J.X. Samuels, and T.A. Joyner. 2021. Ecometric estimation of present and past climate of North America using crown heights of rodents and lagomorphs. Palaeogeography, Palaeoclimatology, Palaeoecology 562:110144. https://doi.org/10.1016/j.palaeo.2020.110144

Short, R.A., S.C. Wallace, and L.G. Emmert. 2019. A New Species of *Teleoceras* (Mammalia, Rhinocerotidae) from the Late Hemphillian of Tennessee. Bulletin of the Florida Museum of Natural History 56(5):183–260.

Shunk, A.J., S.G. Driese, and G.M. Clark. 2006. Latest Miocene to earliest Pliocene sedimentation and climate record derived from paleosinkhole fill deposits, Gray Fossil Site, northeastern Tennessee, USA. Palaeogeography, Palaeoclimatology, Palaeoecology 231(3-4):265–278. https://doi.org/10.1016/j.palaeo.2005.08.001

Shunk, A.J., S.G. Driese, and J.A. Dunbar. 2009. Late Tertiary paleoclimatic interpretation from lacustrine rhythmites in the Gray Fossil Site, northeastern Tennessee, USA. Journal of Paleolimnology 42(1):11–24. https://doi.org/10.1007/s10933-008-9244-0

Siegert, C., and E.J. Hermsen. 2020. *Cavilignum pratchettii* gen. et sp. nov., a novel type of fossil endocarp with open locules from the Neogene Gray Fossil Site, Tennessee, USA. Review of Palaeobotany and Palynology 275:104174. https://doi.org/10.1016/j.revpalbo.2020.104174

Singleton, A. 2021. Terrestrial archives of meteoric ^{10}Be. MS thesis. Purdue University. West Lafayette, IN. 171 pp. https://doi.org/10.25394/PGS.17149166.v1

Singleton, A.A., A.H. Schmidt, P.R. Bierman, D.H. Rood, T.B. Neilson, E.S. Greene, J.A. Bower, and N. Perdrial. 2017. Effects of grain size, mineralogy, and acid-extractable grain coatings on the distribution of the fallout radionuclides ^{7}Be, ^{10}Be, ^{137}Cs, and ^{210}Pb in river sediment. Geochimica et Cosmochimica Acta 197:71–86. https://doi.org/10.1016/j.gca.2016.10.007

Somayajulu, B.L.K. 1967. Beryllium-10 in a manganese nodule. Science 156(3779):1219–1220. https://doi.org/10.1126/science.156.3779.1219

Steadman, D.W. 2011. A Preliminary Look at Fossil Birds from the Gray Fossil Site, Tennessee. Gray Fossil Site 10 Years of Research 73–74.

Tedford, R.H., L.B. Albright III, A.D. Barnosky, I. Ferrusquia-Villafranca, R.M. Hunt, Jr., J.E. Storer, C.C. Swisher III, M.R. Voorhies, S.D. Webb, and D.P. Whistler. 2004. Mammalian biochronology of the Arikareean through Hemphillian interval (late Oligocene through earliest Pliocene epochs). Pp. 169-231, *In* M.O. Woodburne (Ed.). Late Cretaceous and Cenozoic Mammals of North America, Biostratigraphy and Biochronology. Columbia University Press, New York, NY. 363 pp. https://doi.org/10.7312/wood13040-008

U.S. Environmental Protection Agency. 2013. Level III ecoregions of the continental United States: Corvallis, Oregon, U.S. EPA – National Health and Environmental Effects Research Laboratory, map scale 1:7,500,000. https://www.epa.gov/eco-research/level-iii-and-iv-ecoregions-continental-united-states

von Blanckenburg, F., J. Bouchez, and H. Wittmann. 2012. Earth surface erosion and weathering from the ^{10}Be (meteoric)/^{9}Be ratio. Earth and Planetary Science Letters 351:295–305. https://doi.org/10.1016/j.epsl.2012.07.022

Wallace, S.C. 2004. Reconstructing the past: Applications of surveying and GIS to fossil localities. Proceedings of the Annual Meeting for the American Congress on Surveying and Mapping. Tennessee Association of Professional Surveyors 1–12.

Wallace, S.C. 2011. Advanced Members of the Ailuridae (Lesser or Red Pandas – Subfamily Ailurinae). Red Panda 43–60. https://doi.org/10.1016/B978-1-4377-7813-7.00004-5

Wallace, S.C., and L. Lyon. 2022. Systematic revision of the Ailurinae (Mammalia: Carnivora: Ailuridae): With a new species from North America. Red Panda, Second Ed. 31–52. https://doi.org/10.1016/B978-0-12-823753-3.00011-9

Wallace, S.C., and X. Wang. 2004. Two new carnivores from an unusual late Tertiary forest biota in eastern North America. Nature 431(7008):556. https://doi.org/10.1038/nature02819

White, J.M. 2008. Palynodata datafile: 2006 version, with introduction by JM White. In Geological Survey of Canada Open File 5793, 1 CD-ROM.

Whitelaw, J.L., K. Mickus, M.J. Whitelaw, and J. Nave. 2008. High-resolution gravity study of the Gray Fossil Site. Geophysics 73(2):B25–B32. https://doi.org/10.1190/1.2829987

Willenbring, J.K., and F. Von Blanckenburg. 2010. Long-term stability of global erosion rates and weathering during late-Cenozoic cooling. Nature 465(7295):211–214. https://doi.org/10.1038/nature09044

Worobiec, E., Y.C. Liu, and M.S. Zavada. 2013. Palaeoenvironment of late Neogene lacustrine sediments at the Gray Fossil Site, Tennessee, USA. Annales Societatis Geologorum Poloniae 83:51–63.

Worobiec, G., E. Worobiec, and Y.C. Liu. 2018. Fungal remains from late Neogene deposits at the Gray Fossil Site, Tennessee, USA. Mycosphere 9(5):1014–1024. https://doi.org/10.5943/mycosphere/9/5/5

Zobaa, M.K., M.S. Zavada, M.J. Whitelaw, A.J. Shunk, and F.E. Oboh-Ikuenobe. 2011. Palynology and palynofacies analyses of the Gray Fossil Site, eastern Tennessee: Their role in understanding the basin-fill history. Palaeogeography, Palaeoclimatology, Palaeoecology 308(3-4):433–444. https://doi.org/10.1016/j.palaeo.2011.05.051